Structures 59 (2024) 105704

Contents lists available at ScienceDirect

Structures

journal homepage: www.elsevier.com/locate/structures

Component method for bolted SHS end plate splice joints loaded in tension

Rui Yan [a,b,*], Milan Veljkovic [a]

[a] Department of Engineering Structures, Delft University of Technology, Delft, the Netherlands
[b] Department of Civil and Environmental Engineering, The Hong Kong Polytechnic University, Hong Kong, China

ARTICLE INFO

Keywords:
Component method
Yield line
Asymmetric joints
Bolted connection
Square hollow section

ABSTRACT

Bolted end plate connections are traditional solutions for splice joints with square hollow sections (SHS). A cover plate could be used on one side or two adjacent sides of SHS where the end plate is flushed, resulting in two types of asymmetric splice joints. The advantage of the asymmetric joints is that no space is required between the façade panel and the member surface whilst the easy assembly feature remains. The component method is used to design the bolted end plate connection, as stipulated in prEN 1993–1–8. However, the design rule is only available for connections with open cross-sections. In this paper, a modified component method for predicting the tensile resistance (end plate fails with failure mode 1 according to prEN 1993–1–8) and stiffness of the asymmetric bolted SHS end plate splice joints is proposed. First, a parametric study is carried out to develop the component method for the traditional symmetric bolted SHS end plate splices based on the validated finite element (FE) model. Next, a simplified two-dimensional FE model is employed to evaluate the effect of the asymmetric feature on the stiffness of the joint. Finally, a parametric study is carried out on two types of asymmetric joints to validate the interaction model of individual components. The resistance and stiffness of the asymmetric end plate splice joints are well predicted using the modified component method.

1. Introduction

Off-site prefabricated structures have many advantages compared to on-site construction, such as higher quality, less cost, less construction time, and safer worksites. Fast executions require easy connections. Bolted connections are of quick and straightforward assembly, providing an economical and sustainable solution. Hollow sections are widely used in residential and industrial buildings due to the light self-weight, visually attractive shape, excellent torsion resistance and close equivalent stiffness in two main directions. Extensive research has been carried out on innovative bolted hollow section joints in recent years [1–8].

A traditional solution for hollow section splice joints is to weld an end plate to the end of the hollow section off-site and bolt two end plates on-site. Experimental and numerical studies have been carried out on traditional bolted end plate splice joints with bolts placed on two opposite sides or four sides of square hollow sections (SHS) and rectangular hollow sections (RHS) [9–18]. However, the traditional solution requires an installation gap for the end plate between the façade panels and the column surface. Yan et al. [19] proposed two new asymmetric configurations of SHS splice joints, where the end plate is flushed to the SHS profile on one side or two adjacent sides. The new configurations are suitable for columns at the outer corner of a building (corner column splice, labelled CCS) or along the façade (wall column splice, labelled WCS). The advantage of the asymmetric splice joints is that no space is required between the façade panels and the column, whilst the easy assembly feature remains. It has to be emphasised that the column splices are often loaded under compression and/or bending in a real structure. However, to investigate the interaction between different components in the joint, the column splices are tested under tension. The developed component method for the column splices will be further used to predict the bending behaviour of the joint. The splice joint consists of cold-formed SHS tubes, end plates, cover plates, M24 bolts, and M20 bolts, as shown in Fig. 1. Note that a blind (or Hollo) bolt should be used to connect the cover plate and the hollow profile in a real structure.

The component method could predict the resistance and stiffness of bolted end plate connections, as stipulated in prEN 1993–1–8 [20]. Eleven components are involved in predicting CCS and WCS resistance at two critical cross-sections (CS1 and CS2, shown in Fig. 1). Seven components on the cover plate side and three components on the end plate side should be checked at CS1. The seven components on the cover plate side are:

* Corresponding author at: Department of Engineering Structures, Delft University of Technology, Delft, the Netherlands.
E-mail address: cee-rui.yan@polyu.edu.hk (R. Yan).

https://doi.org/10.1016/j.istruc.2023.105704
Received 17 December 2022; Received in revised form 7 November 2023; Accepted 2 December 2023
Available online 12 December 2023

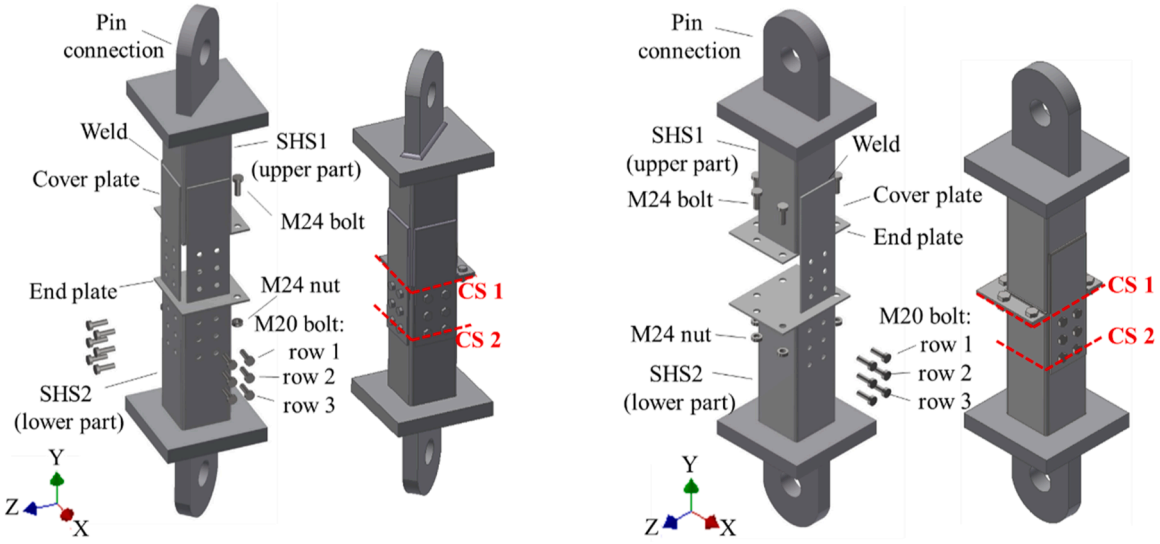

a) Corner column splice (CCS). b) Wall column splice (WCS).

Fig. 1. Two new configurations of splice joint. [19].

a) Layout of corner column splice (CCS). b) Layout of wall column splice (WCS).

Fig. 2. Two types of equivalent T-stub.

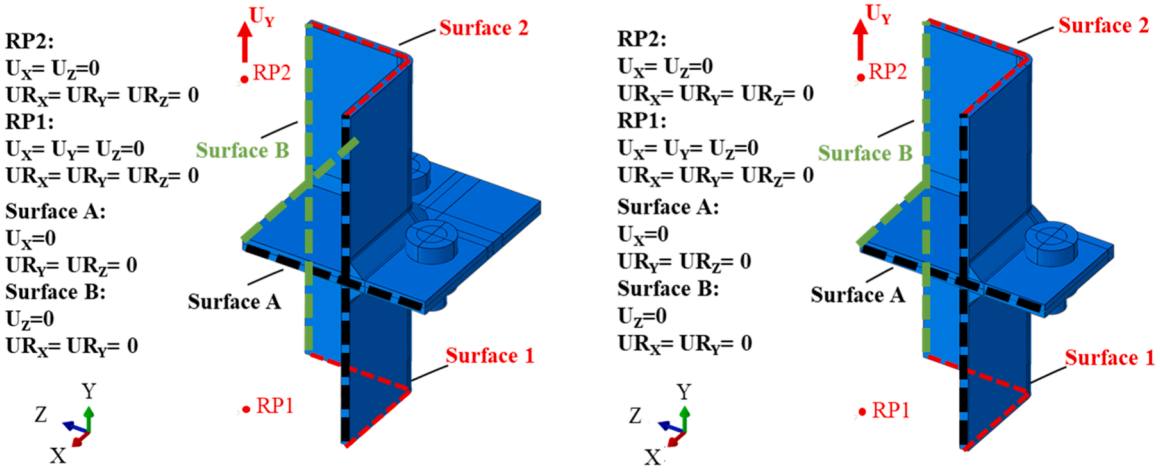

a) Corner T-stub (CT). b) Edge T-stub (ET).

Fig. 3. FEM of two types of T-stub.

1) Plate in tension (cover plate)
2) Bolts in bearing (cover plate)
3) Block tearing failure of the cover plate
4) Bolts in shear
5) Bolts in bearing (column)
6) Block tearing failure of the column
7) Welds (cover plate)

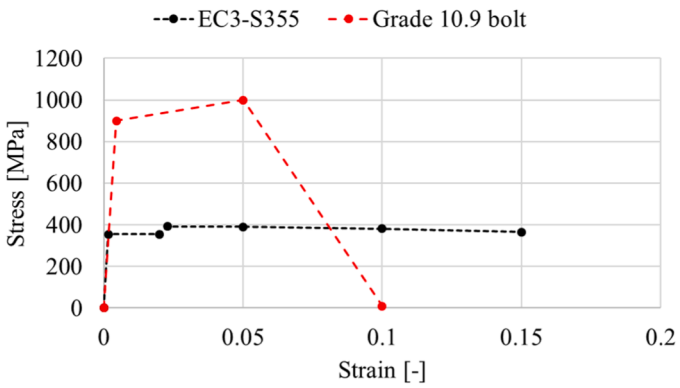

Fig. 4. Engineering stress-strain relationships.

The three components on the end plate side are:

8. End plate in bending
9. Bolts in tension
10. Welds (end plate)

At CS2, the resistance of the whole column cross-section can be calculated using the component plate in tension. The resistance should be verified against the total load of the splice joints.

11. Plate intension (column)

The design rules for all involved components are available in prEN 1993–1–8 [20] except for the component end plate in bending since the effective yield line length equations are suitable for joints with open cross-section members but not hollow section members. Attempts have been made to extend the existing component method to traditional splice joints with RHS and SHS members [9–17]. Yan et al. [19] found that the equations proposed by Steige and Weynand [14] may underestimate the effective yield line length on the end plate, resulting in a rather conservative design resistance.

In this paper, firstly, a parametric study is carried out to develop the component method for the traditional splice joint based on the validated finite element (FE) model. Secondly, the effect of the asymmetric feature on the joint stiffness is evaluated using a 2D FE model. Finally, a modified component method is proposed to predict the resistance and stiffness of CCS and WCS.

2. Parametric study of traditional splice joints

2.1. Finite element (FE) model

Fig. 2 presents the layout of the asymmetric splice joints, from which two types of T-stub: Corner T-stub (CT) and Edge T-stub (ET), are identified. These T-stubs also exist in the traditional splice joints. CT and ET are a quarter of the traditional splice joint with bolts symmetrically positioned on four sides and two sides, respectively. It is worth mentioning that CT is an equivalent T-stub with one bolt row, while ET is only half of an equivalent T-stub with one bolt row.

A parametric study is carried out on identified CT and ET. The FE models of the one-quarter traditional splice joints are presented in Fig. 3. Each model consists of two one-quarter 200 × 8 SHS columns, two end plates, one or two M24 bolts, and two fillet welds with 8.7 mm throat thickness (a_c). The dimensions of the end plate in CT and ET are 200 mm × 200 mm and 100 mm × 200 mm, respectively. The distance between the out surface of SHS and the edge of the end plate is 100 mm.

The S355 nominal mechanical property following the lowest requirements in EN1993–1–1 [21] is assigned to the end plate, the column, and the weld. The nominal mechanical property of grade 10.9 is employed for the bolt. The engineering stress-strain relationships are plotted in Fig. 4. The Young's modulus (E) is 200 GPa for both materials. The commercial software ABAQUS 6.14 [22] is used to conduct the FE analysis. The metal plasticity with the isotropic hardening and von Mises yield criterion is employed.

A hard contact in the normal direction and a tangential contact with

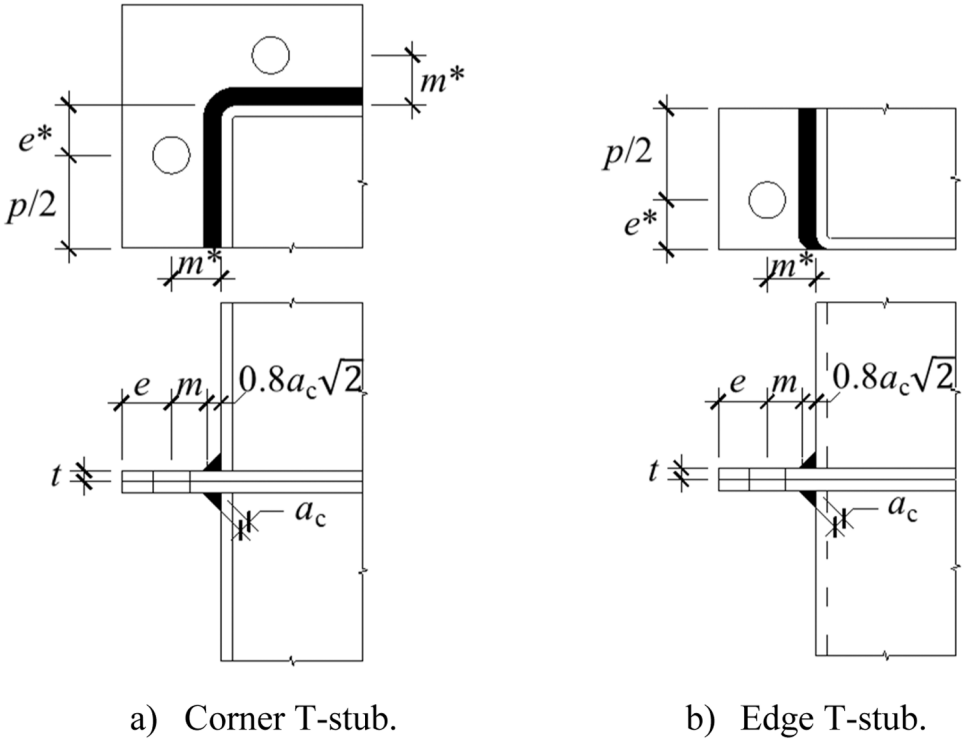

Fig. 5. Dimension symbols of the T-stubs.

Table 1
Investigated parameters [mm].

Parameters	Dimensions						
m^*	35	40	45	50	55	60	65
t	6	8	10				
p	130	100	70				

Table 2
Additional models for the corner T-stub and edge T-stub.

Models	m^* [mm]	t [mm]	p [mm]	Bolt
t6m35M20	35	6	130	M20
t6m35M16	35	6	130	M16
t6m50M20	50	6	130	M20
t6m50M16	50	6	130	M16
t6m65M20	65	6	130	M20
t6m65M16	65	6	130	M16
t6P130	35	6	130	M24
t6P100	35	6	100	M24
t6P70	35	6	70	M24
t8P130	35	8	130	M24
t8P100	35	8	100	M24
t8P70	35	8	70	M24
t10P130	35	10	130	M24
t10P100	35	10	100	M24
t10P70	35	10	70	M24
t12P130	35	12	130	M24

a 0.2 friction coefficient are assigned to the surface-to-surface contact pair. The FEM contains four surface-to-surface contact pairs: the plate to the bolt head and nut contact, the end plate to the end plate contact, the bolt shank to the bolt hole contact, and the tube to the end plate contact. Moreover, the tie constraint is employed to connect the nut to the bolt shank and the fillet weld to the end plate and the tube.

Two reference points RP1 and RP2 are created at the centre of the complete SHS cross-section on the bottom and the top, respectively, as shown in Fig. 3. The reference point is tied to a quarter of the corresponding top or bottom SHS surface, Surface 1 or Surface 2, by Rigid Body constraint. The load is applied at RP2 through a displacement in the Y direction. The rest degrees of freedom at RP1 and RP2 are fully fixed. Symmetric boundary conditions are applied on Surface A and Surface B. Detailed boundary conditions at the surfaces and the reference points are presented in Fig. 3. The model is meshed with the C3D8R element. For all the mesh over the thickness, at least four elements are employed.

Three parameters, which are the end plate thickness (t), the distance from the tube outside surface to the centre of the bolt hole (m^*), and the bolt pitch (p), are investigated in the parametric study. The meaning of each dimension is shown in Fig. 5. Note that e^* is the distance from the centre of the bolt hole to the outer side surface of the hollow section. The range of each parameter is presented in Table 1. 63 models are generated in the parametric study for each T-stub configuration considering all combinations of three parameters. In addition, 16 models for each configuration are generated to verify the derived equations, as presented in Table 2. The first six models, where M20 and M16 bolts are used, verify the effect of the bolt dimension on the joint behaviour. The last ten models have a small end plate with a 70 mm margin between the out surface of SHS and the edge of the end plate (m^*+e). The margin is the same as the experimental dimension in [19]. And the thickness of the end plate varies from 6 mm to 12 mm.

2.2. Identification of the yield pattern

All models fail with the complete yielding of the end plate, which is failure mode 1 of the T-stub model, according to prEN 1993–1–8 [20]. The effective length of the yield line is used to calculate the resistance and stiffness of the T-stub with failure mode 1. The yield line in the end plate of the T-stub model is the boundary of the yield region, implying the location of the plastic hinge. The entire cross-section through the thickness should yield at the plastic hinge. In the FE model, five elements are employed in the thickness direction of the end plate to evaluate the strain level of the end plate's central layer. Fig. 6 explains the reason for using the PEEQ distribution on the central layer of the end plate. The complete end plate is shown on the top (A). A detailed figure on the right (C) presents PEEQ across the thickness for the plate inside the dash rectangular box, which shows the strain state on the edge, but cannot reveal the strain level inside the plate. Alternatively, the PEEQ distribution in the central layer of the end plate (marked by the red solid line in the top figure) is used to demonstrate the region where the complete yielding appears, as shown in the bottom figure (B).

Fig. 7 and Fig. 8 present the equivalent plastic strain (PEEQ) contour plot of the end plate central layer at the load when the maximum PEEQ in the end plate reaches 5%, whilst the maximum PEEQ in other components is lower than 5%. There are two main reasons for using 5% PEEQ as the stop criteria to characterise the yield resistance and the corresponding yield lines. First, 5% PEEQ can be reached by mild steels and high-strength steels before necking. Second, when 5% PEEQ is

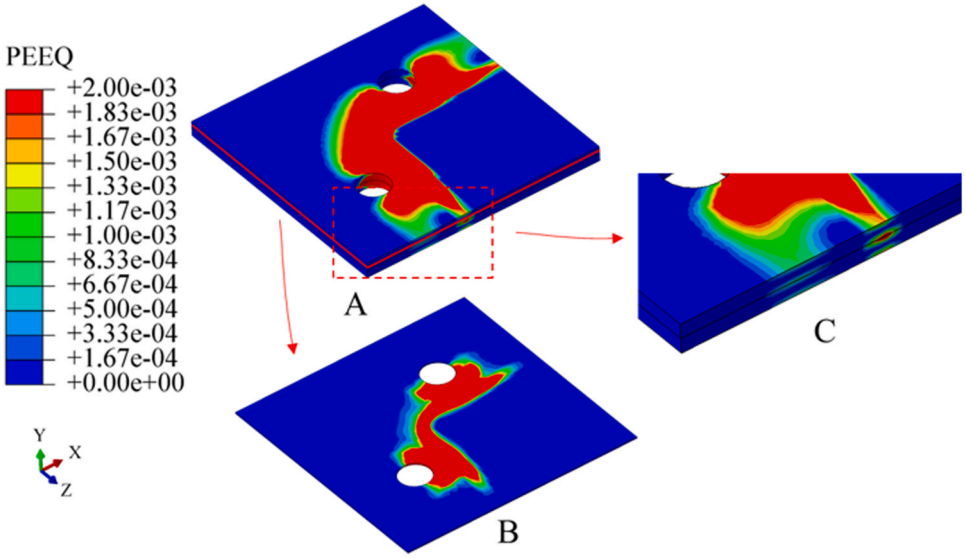

Fig. 6. PEEQ contour plot through thickness.

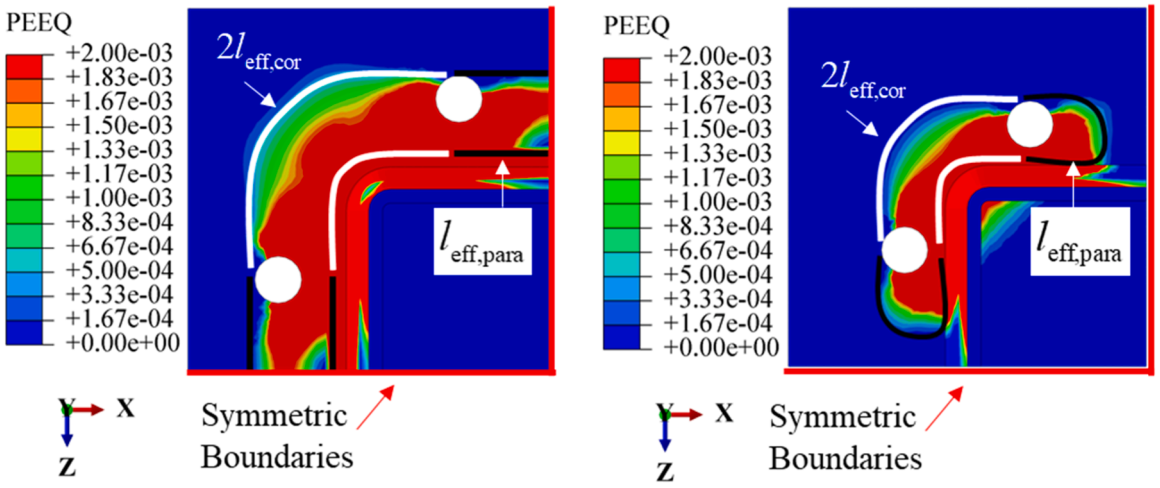

a) Group yield pattern (t=6 mm, m=50 mm, p=100 mm).

b) Individual yield pattern (t=6 mm, m=35 mm, p=130 mm).

Fig. 7. Two typical failure modes of Corner T-stub.

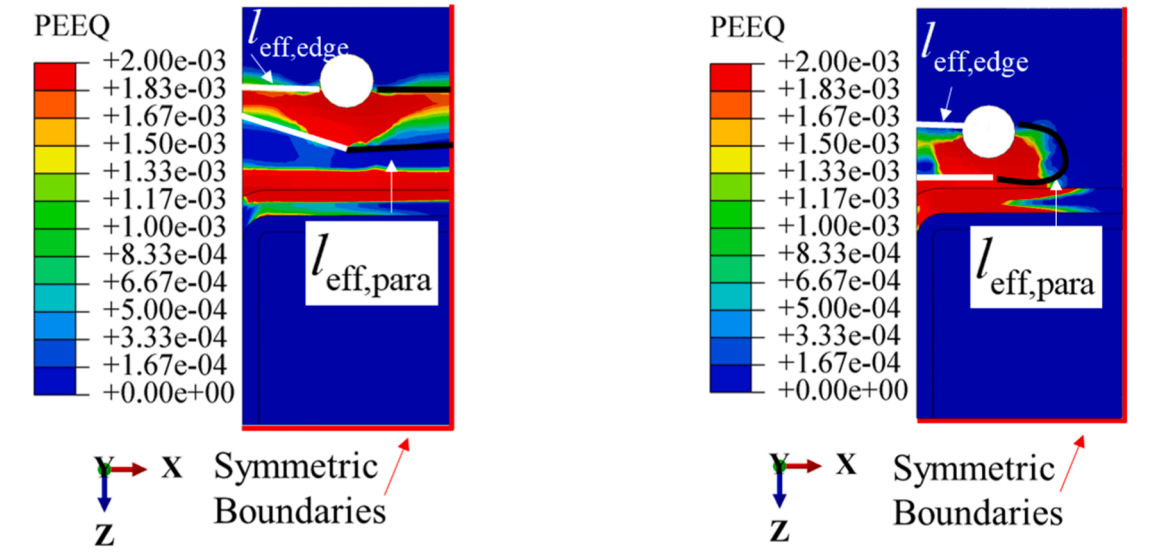

a) Group yield pattern (t=6 mm, m=65 mm, p=100 mm).

b) Individual yield pattern (t=6 mm, m=40 mm, p=130 mm).

Fig. 8. Two typical failure modes of Edge T-stub.

reached in a single element in the end plate, sufficient plastic deformation is developed. If a smaller governing value is used, such as 10 times yield strain ($10\varepsilon_y$), which is often considered as the initiation of strain hardening, the plastic bending moment resistance would only be achieved at the cross-section where $10\varepsilon_y$ is reached, indicating the end plate is not completely yield. The most stressed element where PEEQ reaches 5% is often near the edge of the bolt head/nut or the weld toe at the surface of the end plate. The maximum value in the legend is set to 0.2% to show the yield region. The element in red color means that PEEQ is not less than 0.2%, indicating a complete yielding of the plate through the thickness. As the end plates with different thicknesses show similar yield patterns, only the results of 6 mm end plate are presented to demonstrate the yield pattern.

The material yielding appears at the symmetric boundaries in Fig. 7a) and Fig. 8a), while no plastic deformation is observed at the symmetric boundaries in Fig. 7b) and Fig. 8b). Therefore, two typical yield patterns, which are the group yield pattern and the individual yield pattern concerning two bolts on the same SHS side, could be identified for CT and ET. The yield line on the SHS straight side is presented by the black lines in Fig. 7 and Fig. 8. The type of the yield pattern is identified for all 63 FE models in the parametric study. It is found that a group circular yield pattern tends to appear with an increasing m^*, a decreasing p, and a decreasing t.

Regarding the yield pattern close to the SHS corner, Fig. 7 demonstrates that two bolts close to the same SHS corner fail as a group with a circular yield pattern, which is observed in all FE models. And the

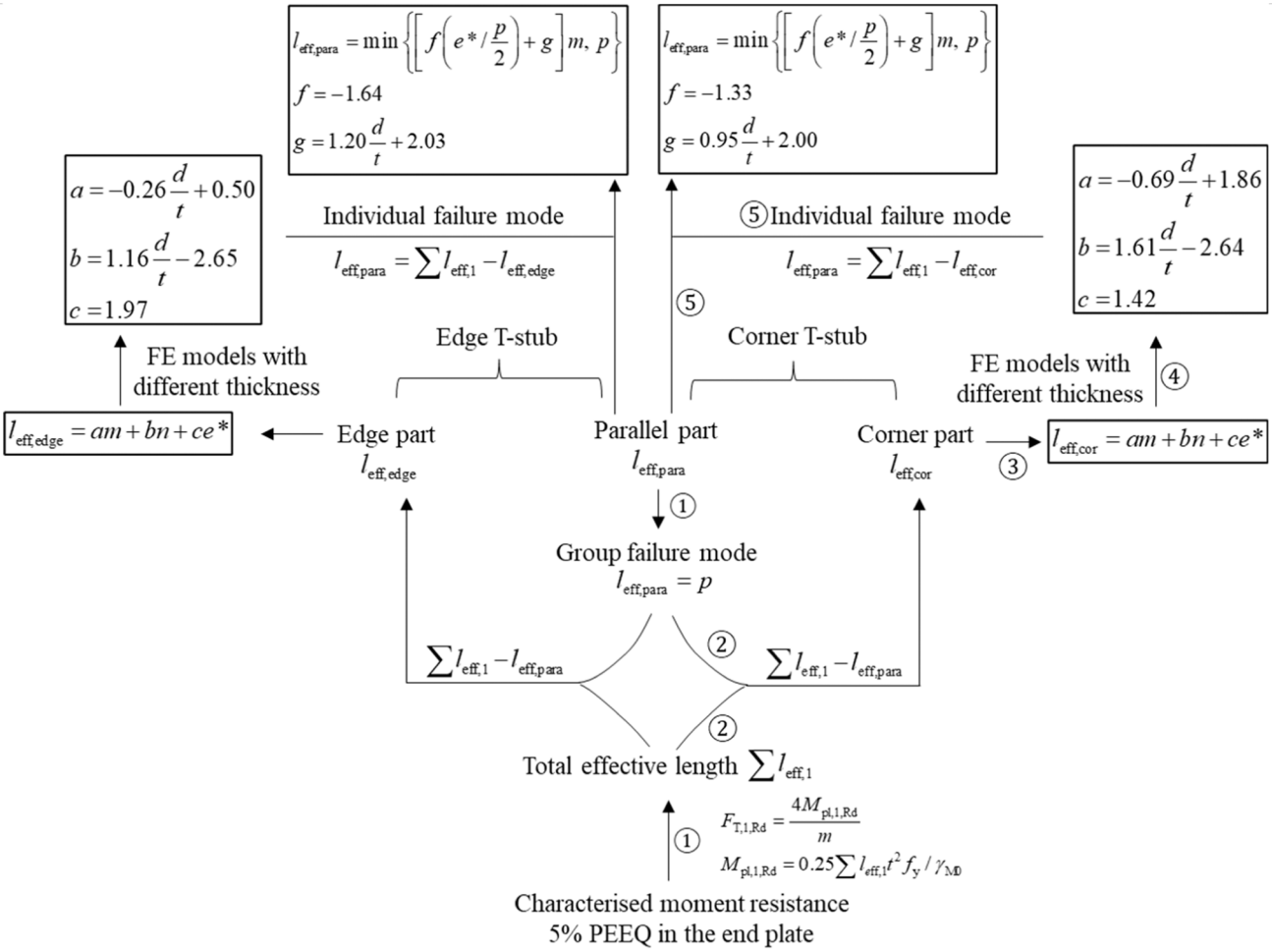

Fig. 9. Flowchart of deriving equations for effective length.

Table 3
Deviation of the predicted effective length.

Type of T-stub		Max [%]	Min [%]	Avg [%]
CT	63 models for derivation	4	-10	-3
	16 models for verification	7	-11	-4
ET	63 models for derivation	5	-15	-2
	16 models for verification	5	-14	-2

Table 4
Deviation of the reduction factor.

Type of T-stub		Max [%]	Min [%]	Avg [%]
CT	63 models for derivation	10	-8	0
	16 models for verification	10	-18	2
ET	63 models for derivation	15	-9	3
	16 models for verification	16	-16	4

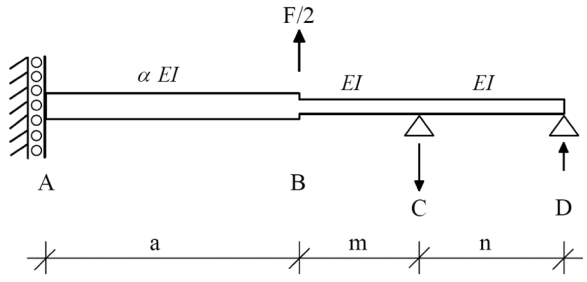

Fig. 10. T-stub stiffness model for bolted RHS end plate in bending.

corresponding yield line is presented by the white lines. For all ET models, it is observed that the yield line (white lines) reaches the edge of the end plate, as shown in Fig. 8. Hence, CT and ET only have one possible yield pattern in the region close to the SHS corner.

2.3. Resistance prediction

Eq. 1 is used to predict the resistance of a T-stub with failure mode 1, according to prEN1993–1–8 [20]. An effective length could be derived if the yield resistance is determined. The yield resistance of CT and ET is determined by the load when the maximum PEEQ in the end plate reaches 5%, whilst the maximum PEEQ in other components are lower than 5%, as illustrated in Section 2.2. Therefore, the effective length is calculated for each FE model in the parametric study.

$$F_{T,1,Rd} = \frac{4M_{pl,1,Rd}}{m}$$
$$M_{pl,1,Rd} = 0.25\sum l_{eff,1} t^2 f_y \Big/ \gamma_{M0} \quad (1)$$

where $\sum l_{eff,1}$ is the effective length of the equivalent T-stub, f_y is the yield strength of the material.

Comparing the FE models using the large and small end plates, 100 mm (e = 65.0 mm, m = 25.2 mm, n = 31.4 mm) and 70 mm (e =

Table 5
Comparison of experimental and predicted resistance.

Specimen	Type	Endplate							Bolt	Resistance [kN]	
		Dimensions [mm]						f_y [MPa]			
		m^*	e	e^*	p	t	a_c			R_u	R_{CM}
31[9]	8	30	30	50	100	6.3	-	352	M20,10.9	630	433
32[9]	8	30	30	50	100	8.8	-	364	M20,10.9	1198	745
A1[23]	4	30	20	15	50	8.0	3.5	464	M16,8.8	267	165
A2[23]	4	30	20	15	50	8.0	3.5	464	M16,8.8	267	165
B1[23]	4	30	20	15	50	10.1	3.5	360	M16,8.8	301	185
B2[23]	4	30	20	15	50	10.1	3.5	360	M16,8.8	290	185

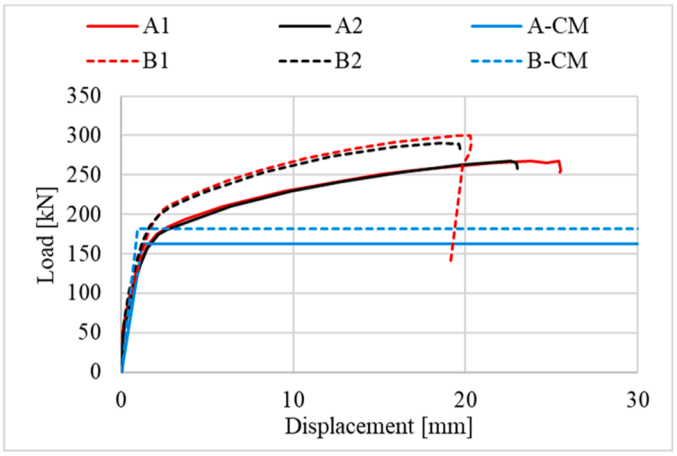

a) Compared to the bi-linear model.

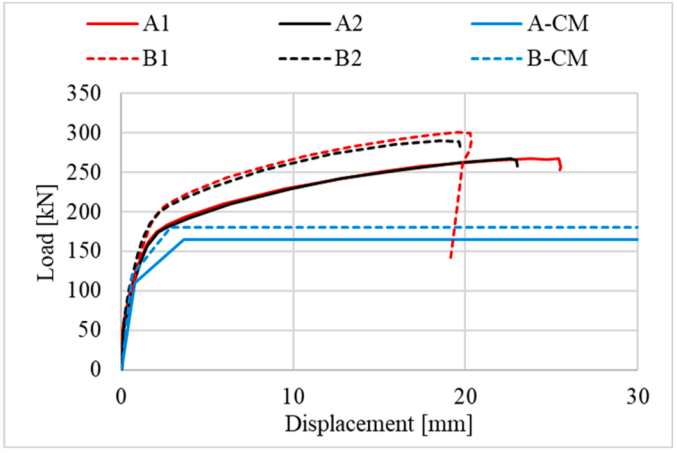

b) Compared to the tri-linear model.

Fig. 11. Load-displacement relationships.

35.0 mm, $m = 25.2$ mm, $n = 31.4$ mm) between the SHS surface and the edge of the end plate, respectively, the load-displacement relationships are identical if the dimensions (except for e) keep the same. As e is already slightly larger than n in the smaller model, and the resistance does not change by increasing e, indicating that the dimension e does not influence the resistance and stiffness when it is larger than 1.25 m. Hence, dimension e, in the effective length equation proposed by prEN1993–1–8 [20], is replaced by dimension n.

A flowchart is presented in Fig. 9 to illustrate the derivation procedures for Eqs. 2 to 5. As CT and ET share the same derivation procedures, CT is employed as an example to elaborate procedures ① to ⑤. The yield line consists of two parts which are the parallel part ($l_{eff,para}$) and the corner part ($l_{eff,cor}$). First, for the FE models with a group failure mode, the effective length of the circular pattern between two bolts on the same SHS side ($l_{eff,para}$, black lines in Fig. 7a) and Fig. 8a)) is the bolt pitch p (two times half bolt pitch), according to prEN1993–1–8 [20]. The total effective length is calculated by Eq. 1. Hence, in the second step, the effective length in the corner ($l_{eff,cor}$, white lines in Fig. 7 and Fig. 8) is calculated by the total lengths subtracting p. In the third step, the key dimensions (m, n, and e^*) for calculating $l_{eff,cor}$ are identified, which are similar to that in prEN 1993–1–8 [20] but replacing e by n. In the fourth step, the values of parameters a, b, and c are determined for a group of FE models with the same end plate thickness. It is found that the d/t ratio influences the value of parameters a and b. Hence, linear equations are proposed for a and b. Since $l_{eff,cor}$ is predictable, $l_{eff,para}$ for the models with individual failure modes on the parallel side can be calculated, which is the total length minus the corner effective length. In the last step, it is found that $l_{eff,para}$ for the individual failure mode strongly depends on m than other dimensions. Besides, the relative position of the bolt to the SHS corner ($e^*/p/2$) and the d/t ratio affect the resistance. Therefore, these four dimensions are involved in calculating a factor which is further used for $l_{eff,para}$ based on m. The calibrated parameters and equations for CT and ET are presented in Eqs. 2 to 5.

Equations for CT:

$$l_{eff,cor} = am + bn + ce*$$
$$a = -0.69\frac{d}{t} + 1.86$$
$$b = 1.61\frac{d}{t} - 2.64 \quad \text{Eq. 2}$$
$$c = 1.42$$

$$l_{eff,para} = \min\left\{\left[f\left(e*\Big/\frac{p}{2}\right) + g\right]m, p\right\}$$
$$f = -1.33 \quad \text{Eq. 3}$$
$$g = 0.95\frac{d}{t} + 2.00$$

Equations for ET:

$$l_{eff,edge} = am + bn + ce*$$
$$a = -0.26\frac{d}{t} + 0.50 \quad \text{Eq. 4}$$
$$b = 1.16\frac{d}{t} - 2.65$$
$$c = 1.97$$

$$l_{eff,para} = \min\left\{\left[f\left(e*\Big/\frac{p}{2}\right) + g\right]m, p\right\}$$
$$f = -1.64 \quad \text{Eq. 5}$$
$$g = 1.20\frac{d}{t} + 2.03$$

where n is min(1.25 m, e); d is the diameter of the bolt; a, b, c, f, and g are coefficients; the rest of the dimensions are visible in Fig. 5.

For the FE models with the individual failure mode, the effective

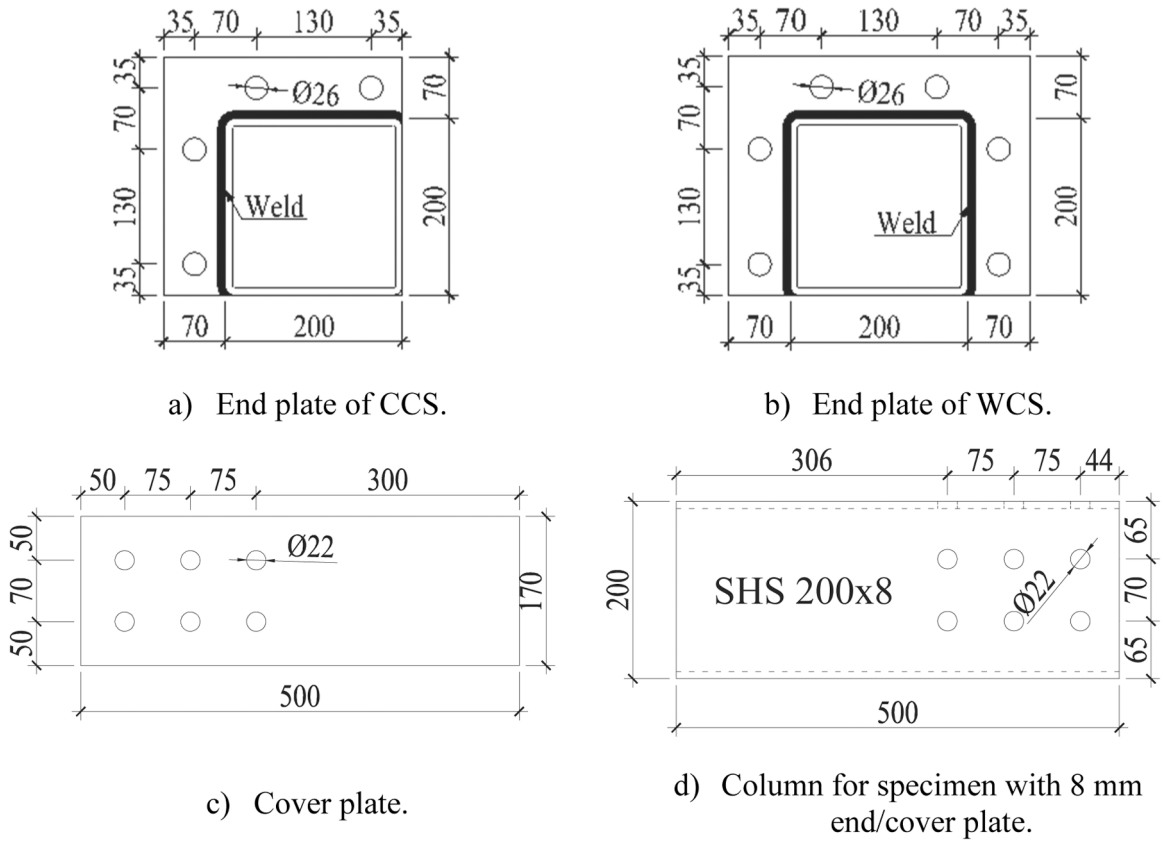

Fig. 12. Dimensions of the experimental configurations.

Table 6
FE models for the parametric study.

FE models		Parameters [mm]			
CCS	WCS	m^*	t	p	R [-]
Ct6m35	Wt6m35	35	6	130	3
Ct6m50	Wt6m50	50	6	130	3
Ct6m65	Wt6m65	65	6	130	3
Ct6p70	Wt6p70	35	6	70	3
Ct6p100	Wt6p100	35	6	100	3
Ct8p70	Wt8p70	35	8	70	3
Ct8p100	Wt8p100	35	8	100	3
Ct6	Wt6	35	6	130	3
Ct8	Wt8	35	8	130	3
Ct10	Wt10	35	10	130	3
Ct12	Wt12	35	12	130	3
Ct6R2	Wt6R2	35	6	130	2
Ct6R1	Wt6R1	35	6	130	1
Ct8R2	Wt8R2	35	8	130	2
Ct8R1	Wt8R1	35	8	130	1
Ct6RM	Wt6RM	35	6	130	3
Ct8RM	Wt8RM	35	8	130	3

length $l_{eff,para}$, black lines in Fig. 7b) and Fig. 8b) is the total effective length obtained from Eq. 1 subtracting the effective length calculated by Eq. 2 (for CT) or Eq. 4 (for ET). Equations for $l_{eff,para}$ with the individual yield pattern are derived for CT and ET, as presented in Eq. 3 and Eq. 5, respectively.

The effective length calculated by the proposed equations is compared to the FE result in Table 3. Considering all FE models, the predicted resistance deviates from the FE results in a range of -15–7%, which is slightly conservative. Hence, the proposed equations could efficiently predict the effective length of failure mode 1. The validated range of the d/t ratio is 2–4.

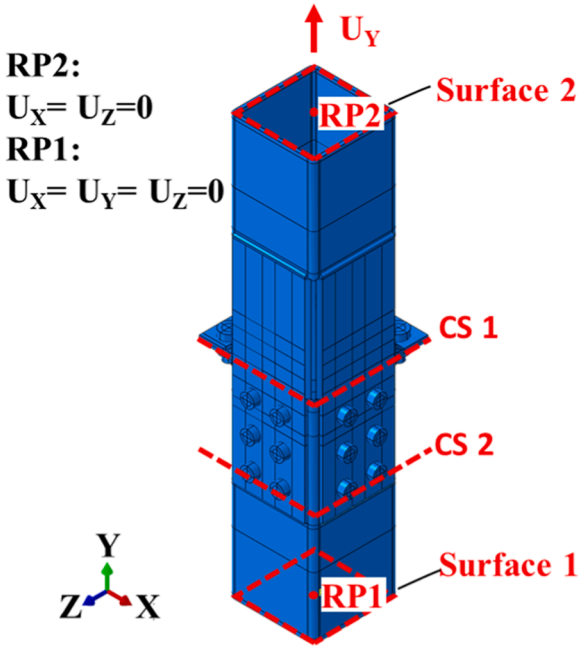

Fig. 13. FE model of CCS.

2.4. Stiffness prediction

Since the T-stub stiffness model in EN1993–1–8 [20] has some unrealistic simplifications regarding the physical boundary conditions, Karlsen and Aalberg [11] proposed a stiffness model for bolted RHS end

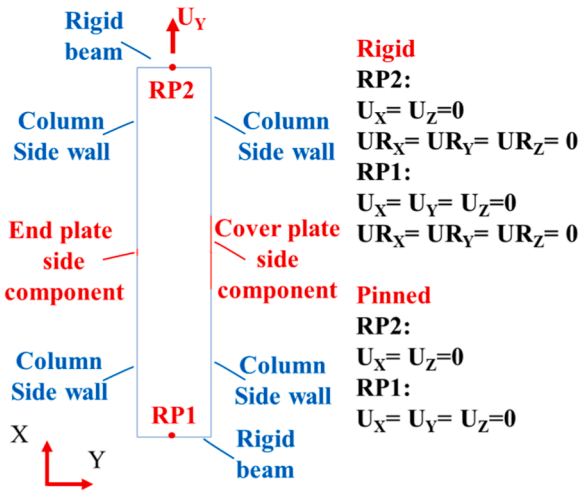

Fig. 14. 2D asymmetric FE model.

Table 7
Stiffness of the 2D FE model with different boundary conditions.

Component stiffness ratio	Stiffness [kN/mm]				Pin/Rigid stiffness ratio
	End plate side	Cover plate side	Rigid	Pin	
0.67	107	160	267	256	0.96
0.5	80	160	240	214	0.89
0.45	72	160	232	200	0.86
0.4	64	160	224	184	0.82
0.33	53	160	213	160	0.75

plate connections, as shown in Fig. 10. The stiffness of the component End plate in bending (k_{ep}) and the component Bolts in tension (k_b) could be calculated by Eq. 6.

$$k_{ep} = \frac{2(3a + 3m\alpha + n\alpha)\cdot l_{eff,ini}\cdot t_p^3}{m^2\left(3m^2\alpha + 4nm\alpha + 12am + 12an\right)}$$
$$l_{eff,ini} = R \times l_{eff} \qquad \text{Eq. 6}$$
$$k_b = \frac{4n(3a + 3m\alpha + n\alpha)}{(6am + 6an + 3m^2\alpha + 2n^2\alpha + 6nm\alpha)}\frac{A_b}{L_b}$$

where a is the distance from the sidewall of the tube to the symmetry line inside the tube; α reflects the 2D bending effect, which increases the stiffness of the end plate inside the tube; $l_{eff,ini}$ is a modified effective length. There are two main reasons for the modification. One is that the effect of the corner region is not considered in the model. Another is that the effective length at the plastic stage is not suitable for the stiffness prediction at the elastic stage. Hence, a factor R is proposed to modify the effective length. The meaning of each dimension is visible in Fig. 10. According to [11], the parameters a and α could be 100 mm and 1, respectively, for traditional splice joints in this study. Since the effective length calculated by the proposed equations (Eq. 2 - Eq. 5) is different from that used in the literature [11], and the effect of the distance from the bolt to the corner is not considered in Eq. 6, the factor R is calibrated based on the parametric study results.

CT and ET consist of three components. Two of the component End plate in bending and one of the component Bolts in tension are connected in tandem. The stiffness equation of CT and ET is presented in Eq. 7. Based on the total stiffness obtained from the FE model and the stiffness of Bolts in tension, the stiffness of End plate in bending (k_{ep}) is calculated using Eq. 7. Consequently, R is determined for each FE model using the calculated effective length and Eq. 6. An equation for predicting R is proposed in Eq. 8. The coefficients h and j are determined for CT and ET separately. The deviation of the predicted reduction factor, consequently the deviation of the predicted stiffness, is presented in Table 4. It can be seen that an acceptable accuracy is achieved by Eq. 8.

$$k_{T-stub} = \frac{1}{\frac{1}{k_{ep}} + \frac{1}{k_b} + \frac{1}{k_{ep}}} \qquad \text{Eq. 7}$$

$$R = h\frac{m}{\sqrt{m^2 + e^{*2}}} + j \qquad \text{Eq. 8}$$

For CT:

$$h = 0.21\frac{d}{t} + 0.24$$
$$j = 0.26\frac{d}{t} - 0.36$$

For ET:

$$h = 0.81$$
$$j = 0.36\frac{d}{t} - 0.62$$

2.5. Verification against experiments in literature

The presented model focuses on failure mode 1 of T-stub – complete yielding of the end plate as stipulated in prEN 1993–1–8 [20]. The experiments with failure mode 1 in literature are used for verification. The

Table 8
CCS resistance.

FEM	Component resistance [kN]									R_{CP} [kN]	R_{EP} [kN]	R_{CM} [kN]
	R_1	R_2	R_3	R_4	R_5	R_6	R_8	R_9	R_{11}			
Ct6m35	237	609	405	588	752	502	133	508	1623	237	133	740
Ct6m50	237	609	405	588	752	502	97	508	1623	237	97	669
Ct6m65	237	609	405	588	752	502	58	508	1623	237	58	591
Ct6p70	237	609	405	588	752	502	134	508	1623	237	134	743
Ct6p100	237	609	405	588	752	502	137	508	1623	237	137	748
Ct8p70	312	802	534	588	741	495	212	508	1623	312	212	1047
Ct8p100	312	802	534	588	741	495	217	508	1623	312	217	1059
Ct6	237	609	405	588	752	502	133	508	1623	237	133	740
Ct8	312	802	534	588	741	495	206	508	1623	312	206	1037
Ct10	395	1015	676	588	735	490	250	508	1623	395	250	1291
Ct12	474	1218	811	588	726	485	313	508	1623	474	313	1574
Ct6R2	237	390	290	392	472	354	133	508	1623	237	133	740
Ct6R1	237	171	175	196	192	207	133	508	1623	171	133	608
Ct8R2	312	514	382	392	461	347	206	508	1623	312	206	1037
Ct8R1	312	225	230	196	182	200	206	508	1623	182	206	775
Ct6RM	347	892	580	588	1123	749	151	508	2071	347	151	997
Ct8RM	439	1127	694	588	1107	738	228	508	2071	439	228	1334

Table 9
WCS resistance.

FEM	Component resistance [kN]										R_{CP} [kN]	$R_{EP,1}$ [kN]	$R_{EP,2}$ [kN]	R_{CM} [kN]
	R_1	R_2	R_3	R_4	R_5	R_6	$R_{8,1}$	$R_{8,2}$	R_9	R_{11}				
Wt6m35	237	609	405	588	752	502	133	140	508	1623	237	133	140	649
Wt6m50	237	609	405	588	752	502	97	106	508	1623	237	97	106	547
Wt6m65	237	609	405	588	752	502	58	61	508	1623	237	58	61	417
Wt6p70	237	609	405	588	752	502	130	133	508	1623	237	130	133	633
Wt6p100	237	609	405	588	752	502	132	137	508	1623	237	132	137	644
Wt8p70	312	802	534	588	741	495	209	212	508	1623	312	209	212	945
Wt8p100	312	802	534	588	741	495	216	219	508	1623	312	216	219	965
Wt6	237	609	405	588	752	502	133	140	508	1623	237	133	140	649
Wt8	312	802	534	588	741	495	206	212	508	1623	312	206	212	942
Wt10	395	1015	676	588	735	490	250	259	508	1623	395	250	259	1163
Wt12	474	1218	811	588	726	485	313	326	508	1623	474	313	326	1439
Wt6R2	237	390	290	392	472	354	133	140	508	1623	237	133	140	649
Wt6R1	237	171	175	196	192	207	133	140	508	1623	171	133	140	583
Wt8R2	312	514	382	392	461	347	206	212	508	1623	312	206	212	942
Wt8R1	312	225	230	196	182	200	206	212	508	1623	182	206	212	811
Wt6RM	347	892	580	588	1123	749	152	159	508	2071	347	152	159	811
Wt8RM	439	1127	694	588	1107	738	228	234	508	2071	439	228	234	1134

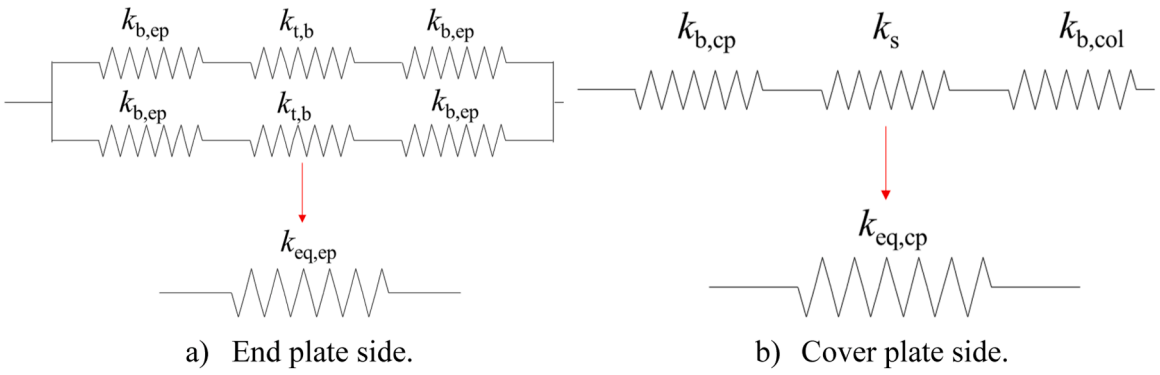

Fig. 15. Equivalent stiffness model.

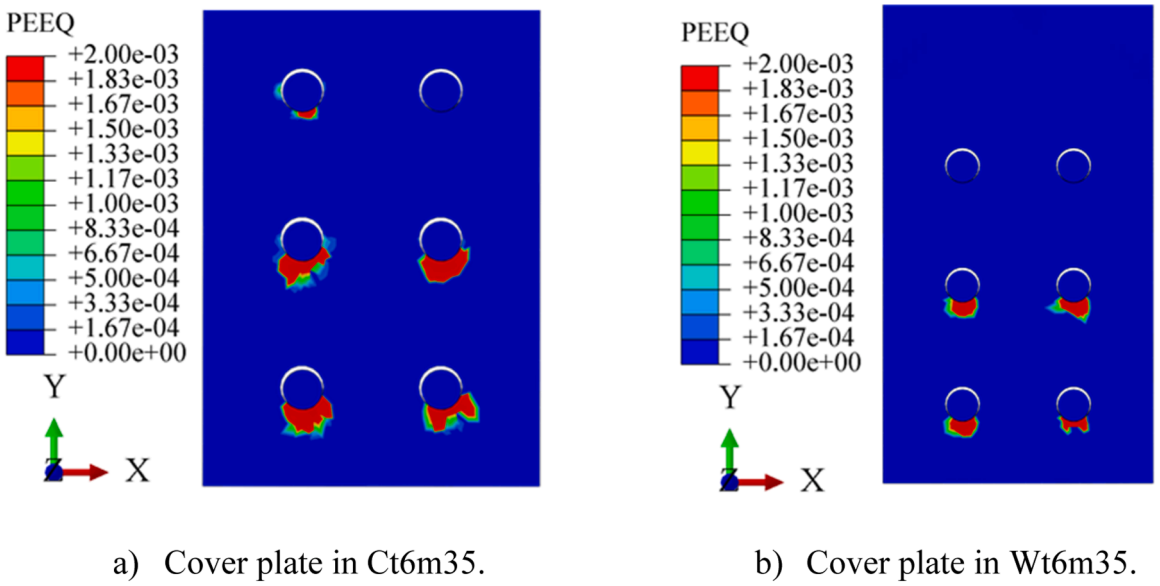

Fig. 16. PEEQ contour plot of the cover plate at the end of the elastic stage.

resistance of two specimens in [9] and four specimens in [23] are predicted by the modified component method and compared to the experimental results in Table 5 and Fig. 11. The number "8" and "4" in the "Type" column represents the joint with eight bolts positioned on four sides and with four bolts symmetrically positioned on two opposite sides, respectively. The measured yield strength shown in Table 5 is used in the component method calculation.

The resistance predicted by the modified component method (R_{CM}) is

Table 10
CCS stiffness.

FEM	$k_{eq,CP}$ [kN/mm]	$k_{eq,EP}$ [kN/mm]	Stiffness ratio $k_{eq,EP}/k_{eq,CP}$	k_{CM} [kN/mm]	k_{FEM} [kN/mm]	k_{CM}/k_{FEM} [-]
Ct6m35	178	207	1.16	564	517	1.09
Ct6m50	178	69	0.39	425	267	1.59
Ct6m65	178	32	0.18	388	208	1.87
Ct6p70	178	196	1.10	552	522	1.06
Ct6p100	178	214	1.20	570	560	1.02
Ct8p70	205	254	1.24	663	629	1.05
Ct8p100	205	286	1.40	696	687	1.01
Ct6	178	207	1.16	564	518	1.09
Ct8	205	294	1.43	704	688	1.02
Ct10	224	338	1.51	786	780	1.01
Ct12	234	390	1.67	859	869	0.99
Ct6R2	152	207	1.36	511	495	1.03
Ct6R1	98	207	2.11	404	455	0.89
Ct8R2	172	294	1.71	639	610	1.05
Ct8R1	96	294	3.06	486	557	0.87
Ct6RM	240	191	0.80	671	587	1.14
Ct8RM	267	291	1.09	824	748	1.10

Table 11
WCS stiffness.

FEM	$k_{eq,CP}$ [kN/mm]	$k_{eq,EP1}$ [kN/mm]	Stiffness ratio $k_{eq,EP1}/k_{eq,CP}$	$k_{eq,EP2}$ [kN/mm]	k_{CM} [kN/mm]	k_{FEM} [kN/mm]	k_{CM}/k_{FEM} [-]
Wt6m35	119	110	0.92	130	489	470	1.04
Wt6m50	119	39	0.33	48	254	214	1.19
Wt6m65	119	17	0.14	23	182	144	1.26
Wt6p70	119	89	0.75	110	427	402	1.06
Wt6p100	119	99	0.83	120	457	477	0.96
Wt8p70	137	123	0.90	152	565	602	0.94
Wt8p100	137	140	1.02	172	620	659	0.94
Wt6	119	110	0.92	130	489	475	1.03
Wt8	137	151	1.10	184	655	706	0.93
Wt10	150	173	1.15	210	743	752	0.99
Wt12	156	199	1.28	242	839	851	0.99
Wt6R2	101	110	1.09	130	471	454	1.04
Wt6R1	66	110	1.67	130	436	396	1.10
Wt8R2	115	151	1.31	184	633	593	1.07
Wt8R1	64	151	2.36	184	582	564	1.03
Wt6RM	160	104	0.65	123	510	487	1.05
Wt8RM	178	147	0.83	178	680	683	1.00

31–38% lower than the experimental ultimate resistance (R_u). Since the load-displacement relationships of the two speicmens in [9] are not available, only four specimens in [11] are presented in Fig. 11 a). It can be seen that the predicted resistance is around the onset of the joint yielding. And the predicted stiffness deviating from the experimental results ranges from − 10% to − 3%. Hence, it can be concluded that the modified component method could effectively predict the tensile behaviour of the bolted end plate SHS joints with the failure mode 1. In addition, prEN 1993–1–8 stipulates that the initial stiffness of a moment resistant joint should be reduced by dividing a stiffness ratio (μ). For the bolted end plate connection, μ approximately equals to 3 if the design load reaches the joint resistance. A tri-linear load-displacement relationship is presented in Fig. 11 b) to show the transition between the elastic part and the plastic plateau. It is worth mentioning that the yield resistance of the FE model is characterised based on the 5% PEEQ criteria, indicating that a limited strain hardening is developed in the end plate. Besides, the employed S355 material model has a low strain hardening behaviour, see Fig. 4. Hence, resistance around the initiation of yielding is predicted, resulting in the gap between the experimental results and the transition between the elastic and plastic stages in the tri-linear relationship. If a higher level of material hardening is involved in the derivation of the prediction model, a higher calculated resistance can be obtained and, consequently, the transition part would match the experimental curve better.

3. Parametric study of asymmetric splice joints

3.1. FE models of splice joints

The parametric study is carried out based on the validated FE model in [19]. Each specimen consists of cold-formed SHS tubes, end plates, cover plates, M24 bolts, and M20 bolts, as shown in Fig. 1. The thickness of the cover plate is the same as the end plate. The column is welded to the end plate with a 9 mm fillet weld. The cover plate is welded to SHS1 with a fillet weld applied on three sides of the cover plate (see Fig. 1). M20 bolts are used to connect the cover plate to SHS2. The nominal dimensions of the experimental configurations are presented in Fig. 12.

The effect of the three parameters m^* , t, and p, referring to Fig. 5, on the tensile behaviour of the asymmetric splice joints is investigated. Additionally, the number of bolt rows ($R = 3, 2, 1$) in the cover plate is also considered. 15 FE models are generated for each splice joint configuration, as shown in Table 6. The dimensions of the FE model in the parametric study is identical to the experimental dimensions, except for the varied parameter. The margin between the SHS out surface and the edge of the end plate (m^*+e) is 70 mm in the experimental configuration. A large end plate with a 100 mm margin is used in FE models Ct6m35, Ct6m50, Ct6m65, Wt6m35, Wt6m50, and Wt6m65.

The same material and the surface contact properties used for CT and ET are employed in the FE models of the asymmetric splice joints. The reference points RP1 and RP2 are tied to Surface 1 and Surface 2, respectively, by the rigid body constraint, as shown in Fig. 13. The load is applied by a displacement at RP2 in the Y direction. The other movements at RP1 and RP2 are fully fixed. A fine mesh (3 mm) is applied on the part where a high plastic strain is expected, while a coarse mesh (9 mm) is used for the less important part to improve the calculation efficiency. The tetrahedral C3D10M element is used for the transition part, connecting the fine mesh part and the coarse mesh part. The C3D8R element is used for the rest part of the model. For all the mesh over the thickness, at least four elements are employed.

3.2. 2D asymmetric FE model

The splice joint consists of several individual components on each SHS side, as illustrated in Section 1. The resistance of the splice joint is determined by the sum of the governing resistances on four SHS sides regardless of the asymmetric feature, according to [19]. The equivalent stiffness of one SHS side depends on the stiffness and the interaction of the individual components, indicating that the stiffness may vary from side to side. Consequently, a question arises on whether the stiffness of the splice joints is the sum of the equivalent stiffness of four sides. Therefore, a simplified 2D FE model is employed to evaluate the influence of the stiffness ratio of two opposite sides on the stiffness of the splice joint.

The 2D FE model contains two vertical columns and two horizontal rigid beams, as shown in Fig. 14. The height and the width of the model are 1000 mm and 200 mm, respectively, which are the same as the splice joint dimensions. The rigid beam and the rigid connection between the beam and the column are employed to satisfy the plane section assumption in the SHS cross-section. Each column consists of three segments, corresponding to three parts in the 3D splice joint. The top and bottom column segments in blue represent the SHS sidewall, which has an infinite tensile stiffness according to prEN 1993–1–8 [20]. The middle red segment (beam element) in each column represents the equivalent component on the end plate side and the cover plate side. The equivalent component on the end plate side includes two End plate in bending components and one Bolts in tension component, which are connected in tandem. Since the investigated end plate thickness is around 10 mm, a constant 20 mm length is used for the middle segment

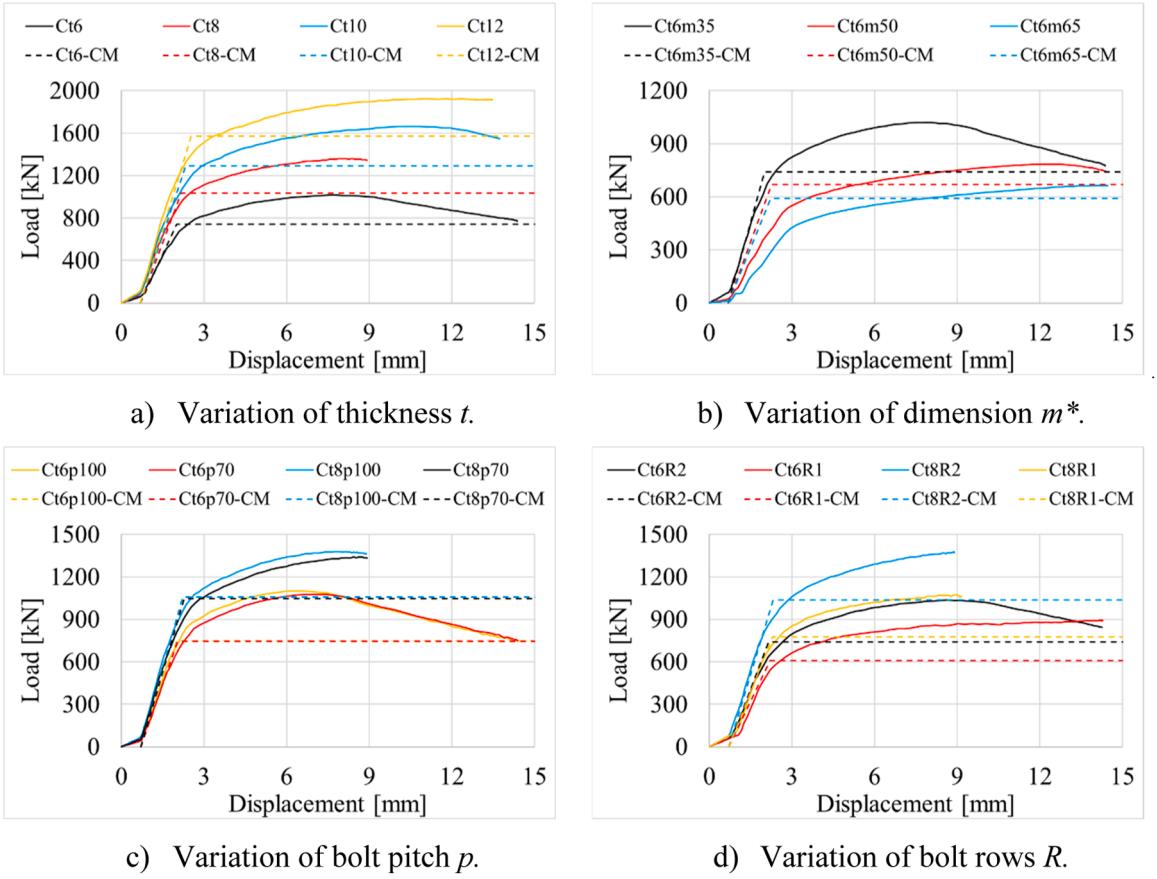

Fig. 17. Comparison for CCS.

on the end plate side. On the cover plate side, the equivalent component comprises two Bolts in bearing components and one Bolts in shear component connecting in tandem. These components exist in a region around 200 mm long. Therefore, the middle segment on the cover plate side is 200 mm.

The equivalent stiffness is calculated and assigned to the middle segment of the cover plate side based on the Wt6 specimen. On the end plate side, a reduced equivalent stiffness, which varies from 2/3 to 1/3 equivalent stiffness of the cover plate side, is used for the middle segment in order to investigate the effect of the stiffness ratio of two sides on the splice joint stiffness.

Since the boundary of the splice joint is an intermediate condition between the rigid and pin constraints in the real structure, these two boundary conditions are used as the upper and lower bound in the 2D FE model. The load is applied by a displacement in the Y direction at RP2. Details of the boundary conditions are shown in Fig. 14.

Table 7 presents the stiffness of the 2D FE model with different boundary conditions (Rigid and Pin). The component stiffness ratio is the equivalent stiffness of the end plate side over the cover plate side. It can be seen that the total stiffness equals the sum of the stiffness on two sides if the rigid boundary condition is applied, while the model with the pin boundary condition has a lower stiffness. Moreover, the Pin/Rigid stiffness ratio decreases more significantly with a lower component stiffness ratio, indicating that the secondary bending is more pronounced if a significant stiffness difference exists between two opposite sides. The stiffness difference between models with pin and rigid boundary conditions is less than 11% when the stiffness ratio is larger than 0.5. Therefore, a lower bound of 0.5 (consequently an upper bound of 2) is proposed for the component stiffness ratio to limit the secondary bending phenomenon. A satisfactory stiffness, with less than 11% deviation, could be obtained by summing up the equivalent stiffness on four SHS sides, provided that the component stiffness ratio ranges from 0.5 to 2.

3.3. *Resistance prediction*

The component method is used to predict the splice joint resistance in this subsection and the stiffness in the next subsection. Eleven individual components are involved in the resistance prediction, as illustrated in Section 1. The predicted resistances of the individual components (R_1–R_{11}) are shown in Table 8 and Table 9 for CCS and WCS, respectively. The nominal yield strength 355 MPa which is the yield strength of the material model used in the FE analysis is used in the calculation. The suffixes 1–11 are related to the component number used in Section 1. In Table 9, suffixes ",1" and ",2" are used to denote the SHS side opposite and adjacent to the cover plate side, respectively. Note that the weld is designed as a full-strength weld, and the resistance is not presented in the table. The formulas for the employed components are summarised in Appendix A.

The resistances of the cover plate side (R_{cp}) and the end plate side (R_{ep}) are governed by the lowest resistance among the components on each side. It is worth mentioning that the parameter α in the stiffness model, referring to Eq. 6, is 1 for the end plate sides adjacent to the cover plate side in WCS, while α is 0 in other cases since the cover plate side cannot constrain the end plate inside the tube. The resistance of the critical cross-Section 1 (CS1), depicted in Fig. 1, is the sum of the resistance of four sides. The resistance of the critical cross-Section 2 (CS2) depends on the resistance of the column net cross-section with two bolt holes (R_{11}). Hence, the splice joint resistance predicted by the component method (R_{CM}) is the lower resistance of two critical cross-sections.

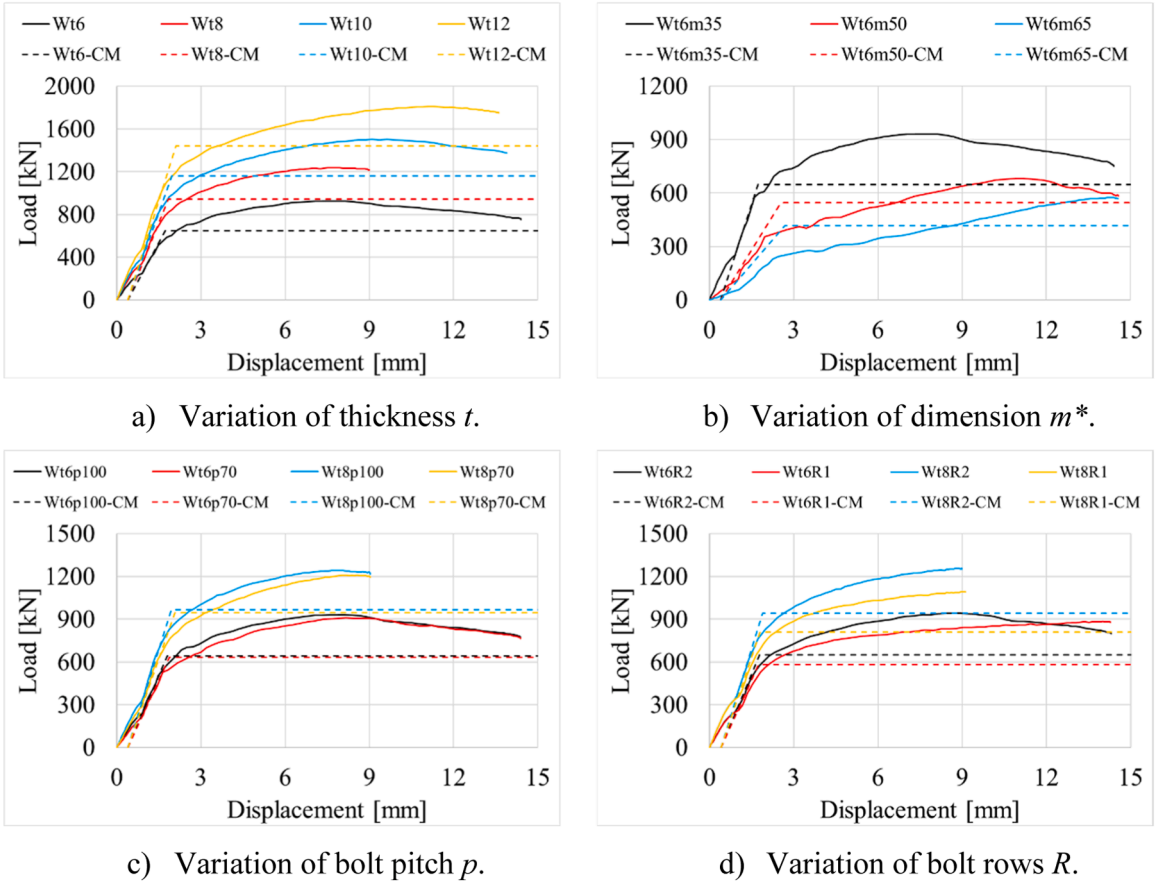

a) Variation of thickness *t*. b) Variation of dimension *m**.

c) Variation of bolt pitch *p*. d) Variation of bolt rows *R*.

Fig. 18. Comparison for WCS.

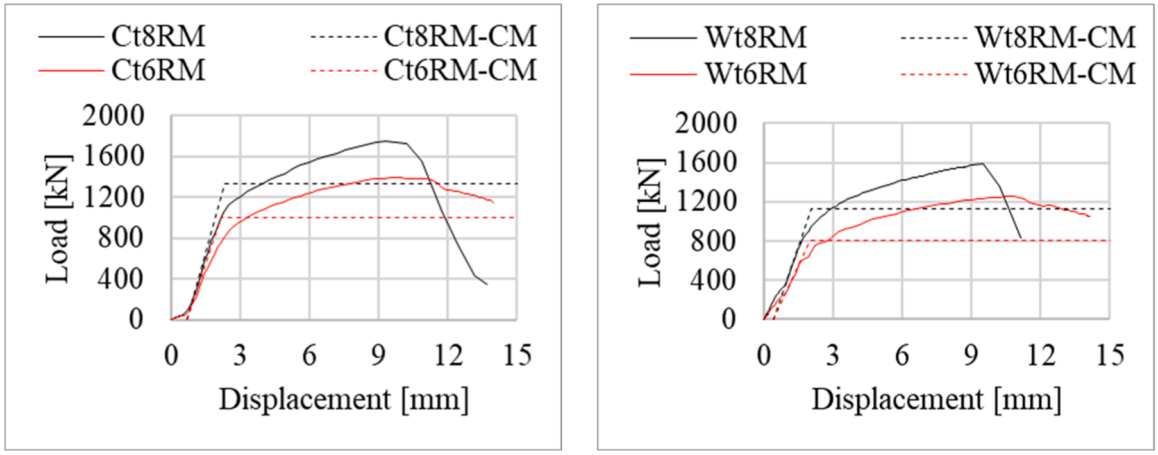

a) CCS. b) WCS.

Fig. 19. Comparison of validated experiments.

3.4. *Stiffness prediction*

The splice joint stiffness is calculated by summing up the equivalent stiffness of four SHS sides, provided that the stiffness ratio of opposite sides ranges between 0.5 and 2. The equivalent stiffness of the end plate side ($k_{eq,ep}$) depends on the components End plate in bending ($k_{b,ep}$) and Bolts in tension ($k_{t,b}$) which are connected in tandem, as shown in Fig. 15 a). Note that two spring rows interact in parallel for one end plate side, as each side contains two bolts. On the cover plate side, three components which are Bolts in bearing for the cover plate ($k_{b,cp}$), Bolts in shear (k_s), and Bolts in bearing for the column ($k_{b,col}$) should be considered in the equivalent stiffness ($k_{eq,cp}$) calculation. Fig. 15 b) presents the tandem interaction of those three components.

Two methods for predicting the stiffness of the component Bolts in bearing are provided in prEN 1993–1–8 [20]. The non-dimensional bearing stress method is adopted in this study. The formulas are presented in Eq. 9.

$$k_b = \frac{\overline{S}_b n t_j f_u}{E} \qquad \overline{\sigma}_{b,Ed} = \frac{F_{v,Ed}}{d t_j f_u}$$
$$\overline{S}_b = \frac{\overline{\sigma}_{b,Ed}}{\frac{u}{d}\left(\overline{\sigma}_b = \overline{\sigma}_{b,Ed}\right)} \qquad \overline{\sigma}_b = \frac{126u/d}{\left(1+\sqrt{30u/d}\right)^2} \qquad \text{Eq. 9}$$

where n is the number of bolts; f_u is the ultimate tensile strength of the steel plate to which the bolt bears; t_j is the thickness of the plate component; $\overline{S}_b$is the relative bearing stiffness; $\overline{\sigma}_{b,Ed}$ is the non-dimensional average bearing stress; $u/d(\overline{\sigma}_b = \overline{\sigma}_{b,Ed})$ is the non-dimensional bolt hole elongation at non-dimensional design bearing stress; u is the bolt hole elongation; d is the bolt diameter; $\overline{\sigma}_b$ is the non-dimensional average bearing stress; $F_{v,Ed}$ is the design shear force per bolt which equals to the design resistance on the cover plate side divided by the number of bolts.

Due to the clearance of the bolt hole in the cover plate and the tube, the cover plate is not activated at the beginning, indicating that the initial stiffness entirely attributes to the bolted end plate connection. After the slip of the cover plate, the components on the cover plate side are gradually activated and contribute to the splice joint stiffness. However, due to the asymmetric feature, the number of bolts that contributes to the elastic stiffness of the cover plate side is vague. Fig. 16 depicts the PEEQ contour plots of the cover plate in Ct6m35 and Wt6m35 at the end of the elastic stage. It can be seen that the plastic strain does not appear in some of the bolt holes, indicating that a reduced number of bolts should be used to calculate the stiffness of the cover plate side.

The equivalent stiffness of the cover plate side is measured from the FE models based on the local deformation on the cover plate side and the load transferred by the cover plate. Considering the number of activated bolts, an activation factor 0.75 and 0.5, which is used to reduce the equivalent stiffness of the cover plate side, is proposed for CCS and WCS, respectively. The predicted and the FE results are compared in Table 10 and Table 11. The prediction deviates in a range of 0.87–1.09 and 0.93–1.10 for CCS and WCS, respectively. Note that the models with 50 mm and 65 mm m^* are excluded from the discussion since the stiffness ratio $k_{eq,EP}/ k_{eq,CP}$ is out of the bound (0.5–2). It is worth mentioning that the employed analytical model in Fig. 15 b) and the activation factor are a compromise solution for the cover plate connection, which cannot capture the detailed load distribution and non-linear behaviour in each bolt. A more realistic model proposed by Henriques et al. [24] should be used to model the lap plate connection for further improvement.

3.5. Load-deformation relationships

The load-displacement relationships predicted by the component method are compared to the FE results in Fig. 17 and Fig. 18. In addition to the 15 FE models in the parametric study, the results of the FE models validated against the experiments in [19] are also presented in Table 8–Table 11, and Fig. 19, with the suffix 'RM'. The material yield strength measured from tensile coupon tests is used in the validation of the analytical model against the experiments. Detailed material strength and the dimensions of the specimens can be found in [19]. Note that the 'CM' curves of the Corner and Wall column splice are offset for 0.7 mm and 0.4 mm, respectively, in order to compare the stiffness visually. The results in Figs. 17–19 show that the component method predicts a resistance around the onset of the joint yielding. And the stiffness of the FE model after the initial slip of the cover plate is well predicted by the component method.

4. Conclusions

Two types of T-stub, namely Corner T-stub (CT) and Edge T-stub (ET), are identified from the proposed asymmetric Corner column splice (CCS) and Wall column splice (WCS). CT and ET are one-quarter of the traditional splice joints with bolts positioned on four sides and two opposite sides of SHS, respectively. Based on the validated FE models for CCS and WCS, a parametric study is conducted on CT and ET. Equations are proposed to predict the resistance (end plate fails with failure mode 1 according to prEN 1993–1–8) and stiffness of the symmetric splice joints. Next, the effect of the stiffness difference on the opposite sides of the joint is evaluated by a simplified 2D FEM. Finally, a parametric study is carried out on CCS and WCS. The resistance (end plate fails with failure mode 1) and stiffness predicted by the modified component method match the FE results well. Based on the presented results, the following conclusions are drawn.

1. Compared to the characterised yield resistance (corresponding to 5% PEEQ in the end plate), the predicted resistance of CT and ET deviates in a range of -15–7% with an average -3% deviation, including all FE models. A factor R is calibrated for the effective length in the CT and ET stiffness prediction. The modified component method predicts a stiffness deviating from the FE results in a range of -18–16%. And the range is -10 −3% compared to the tested joint in the literature.
2. A stiffness ratio (0.5–2) between the opposite sides of SHS is proposed in order to limit the secondary bending. The deviation of the predicted stiffness (sum of the stiffness on two sides) is less than 11%.
3. A limited number of bolts in the cover plate are activated at the end of the elastic stage. An activation factor is proposed for reducing the equivalent stiffness of the cover plate side, considering the effect of the bolt clearance in the cover plate and the tube. The factors are 0.75 and 0.5 for CCS and WCS, respectively.
4. Regardless of the model with stiffness ratio out of the bound (0.5–2), the modified component method predicts the stiffness deviating from the FE results in a range of -13–14% and -7–10% for CCS and WCS, respectively.

Declaration of Competing Interest

The authors declare that they have no known competing financial interests or personal relationships that could have appeared to influence the work reported in this paper.

Acknowledgements

The research presented in this paper is based on the results of the INNO3DJOINTS project. The work was supported by the RFCS [grant numbers 749959]. The financial support is thereby gratefully acknowledged.

Appendix

Appendix A Design formulas for the employed components

- Plate in tension (R1, R11) prEN 1993–1–1:2020, Clause 8.2.3

$$N_{t,Rd} = \min\left(\frac{A_g f_y}{\gamma_{M0}}; \frac{A_{net} f_u}{\gamma_{M2}}\right)$$

where A_g and A_{net} are the gross area and the net area of the cross section, respectively. f_y and f_u are the yield and ultimate resistance of the plate, respectively. γ_{M0} and γ_{M2} are the partial factors equals to 1.0 and 1.25, respectively.

- Bolts in bearing (R2, R5) prEN 1993–1–8:2021, Clause 5.7

$$F_{b,Rd} = \frac{k_m \alpha_b f_u d t}{\gamma_{M2}}$$

$$-\text{for end bolts}: \ \alpha_b = \min\left(\frac{e_1}{d_0}; 3\frac{f_{ub}}{f_u}; 3\right)$$

$$-\text{for inner bolts}: \ \alpha_b = \min\left(\frac{p_1}{d_0} - \frac{1}{2}; 3\frac{f_{ub}}{f_u}; 3\right)$$

$$k_m = 1 \text{ for steel grade lower than S460, otherwise, } k_m = 0.9$$

where f_{ub} is the ultimate resistance of the bolt. e_1 is the distance from the bolt centre to the edge of the plate. d_0 is the diameter of the bolt hole. p_1 is the bolt pitch along the loading direction.

- Block tearing failure of the cover plate (R3, R6) prEN 1993–1–8:2021, Clause 5.10

$$V_{eff,1,Rd} = \left[A_{nt} f_u + \min\left(\frac{A_{gv} f_y}{\sqrt{3}}; \frac{A_{nv} f_u}{\sqrt{3}}\right)\right] \Big/ \gamma_{M2}$$

where A_{nt} and A_{gv} are the net area and the gross area subjected to tension, respectively.

- Bolts in shear (R4) prEN 1993–1–8:2021, Clause 5.7

$$F_{v,Rd} = \frac{\alpha_v f_{ub} A_s}{\gamma_{M2}}$$

$$-\text{for property classes 4.6, 5.6 and 8.8}: \ \alpha_v = 0.6$$

$$-\text{for property classes 4.8, 5.8, 6.8 and10.9}: \ \alpha_v = 0.5$$

where A_s is the tensile stress area of the bolt.

- Bolts in tension (R9) prEN 1993–1–8:2021, Clause 5.7

$$F_{t,Rd} = \frac{0.9 f_{ub} A_s}{\gamma_{M2}}$$

References

[1] Li GQ, Liu K, Wang YB, Dai Z. Moment resistance of blind-bolted SHS column splice joint subjected to eccentric compression. Thin-Walled Struct 2019;141:184–93. https://doi.org/10.1016/j.tws.2019.04.015.

[2] Mahmood M, Tizani W. A component model for column face in bending of extended HolloBolt connections. J Constr Steel Res 2021;182:106655. https://doi.org/10.1016/j.jcsr.2021.106655.

[3] Wang P, Sun L, Zhang B, Yang X, Liu F, Han Z. Experimental studies on T-stub to hollow section column connection bolted by T-head square-neck one-side bolts under tension. J Constr Steel Res 2021;178:106493. https://doi.org/10.1016/j.jcsr.2020.106493.

[4] He R, Shu X, Zhang Z. Experimental study on the tensile performance of high-strength blind-bolted T-stub with endplate tapping. J Eng Sci Technol Rev 2018;11:109–18. https://doi.org/10.25103/jestr.115.13.

[5] D'Antimo M, Demonceau JF, Jaspart JP, Latour M, Rizzano G. Experimental and theoretical analysis of shear bolted connections for tubular structures. J Constr Steel Res 2017;138:264–82. https://doi.org/10.1016/j.jcsr.2017.07.015.

[6] Roquete L, Oliveira MM de, Sarmanho AMC, Xavier EM, Alves VN. Behavior and design formulation of steel CHS with sleeve connections. J Constr Steel Res 2021;177:106465. https://doi.org/10.1016/j.jcsr.2020.106465.

[7] Chen Z, Liu J, Yu Y. Experimental study on interior connections in modular steel buildings. Eng Struct 2017;147:625–38. https://doi.org/10.1016/j.engstruct.2017.06.002.

[8] Sadeghi SN, Heidarpour A, Zhao XL, Al-Mahaidi R. A component-based model for innovative prefabricated beam-to-hybrid tubular column connections. Thin-Walled Struct 2018;132:265–75. https://doi.org/10.1016/j.tws.2018.08.021.

[9] Kato B, Mukai A. Bolted tension flanges joining square hollow section members. J Constr Steel Res 1985;5:163–77. https://doi.org/10.1016/0143-974X(85)90001-X.

[10] Willibald S. Bolted connections for rectangular hollow sections under tensile loading. Karlsr Inst Technol 2003. https://doi.org/DOI:10.5445/IR/1672003.

[11] F. Torp, K. Faglaerer,: Førsteamanuensis, A. Aalberg, Bolted Rhs End-Plate Joints in Axial Tension, in: Nordic Steel Construction Conference, Oslo, 2012. https://doi.org/http://hdl.handle.net/11250/228203.

[12] Packer JA, Bruno L, Birkemoe PC. Limit analysis of bolted RHS flange plate joints. J Struct Eng 1989;115:2226–42. https://doi.org/10.1061/(asce)0733-9445(1989)115:9(2226).

[13] B. Kato, A. Mukai, Bolted tension flanges joining square hollow section members-Supplement: Bolted at two sides of flange, CIDECT Program 8C Rep. No. 8C-85/10-E, 1985.

[14] Steige Y, Weynand K. Design resistance of end plate splices with hollow sections. Steel Constr 2015;8:187–93. https://doi.org/10.1002/stco.201510023.

[15] K. Weynand, J.-P. Jaspart, J.F. Demonceau, L. Zhang, Component method for tubular joints, CIDECT Report 16F – 3/15, Final Report, 2015.

[16] Hilkka Ronni; Markku Heinisuo, Test Report, End Plate Joints of Steel Tubes, Biaxial and Weak Axis Bending, Tampere, 2010. https://doi.org/https://urn.fi/URN:NBN:fi:tty-2011121314930.

[17] Wheeler AT, Clarke MJ, Hancock GJ, Murray TM. Design model for bolted moment end plate connections joining rectangular hollow sections. J Struct Eng 1998;124:164–73. https://doi.org/10.1061/(ASCE)0733-9445(1998)124:2(164).

[18] Heinisuo M, Ronni H, Perttola H, Aalto A, Tiainen T. End and base plate joints with corner bolts for rectangular tubular member. J Constr Steel Res 2012;75:85–92. https://doi.org/10.1016/j.jcsr.2012.03.013.

[19] Yan R, Xin H, Veljkovic M, da Silva LS. Tensile behaviour of asymmetric bolted square hollow section column splices. Thin-Walled Struct 2023;190:111014. https://doi.org/10.1016/j.tws.2023.111014.

[20] CEN, prEN 1993–1-8:2021 - Design of steel structures - Part 1–8: Design of joints (draft of EN1993–1-8: 2021), (2022).

[21] CEN, prEN 1993–1-1:2020 - Design of steel structures - Part 1–1: General rules and rules for buildings (draft of EN1993–1-1: 2020), (2021).

[22] ABAQUS, Abaqus Analysis User's Manual, 6.14 version, (2014).
[23] Karlsen FT. Joints for elements of hollow sections. Nor Univ Sci Technol 2011. ⟨http://hdl.handle.net/11250/236792⟩. accessed September 22, 2023.
[24] Henriques J, Jaspart J-P, Simões Da Silva L. Ductility requirements for the design of bolted lap shear connections in bearing. Adv Steel Constr 2014;10:33–52. ⟨https://www.researchgate.net/publication/289362925⟩.